Technological University Dublin
ARROW@TU Dublin

Articles | Photonics Research Centre

2019

Ultrabroadband mid-infrared emission from Cr 2+ -doped infrared transparent chalcogenide glass ceramics embedded with thermally grown ZnS nanorods

Xiaosong Lu
Harbin Engineering University

Zhiqiang Lai
Harbin Engineering University

Runan Zhang
Harbin Engineering University

See next page for additional authors

Follow this and additional works at: https://arrow.tudublin.ie/prcart

 Part of the Electrical and Computer Engineering Commons, Engineering Physics Commons, and the Optics Commons

Recommended Citation

Xiaosong Lu, Zhiqiang Lai, Runan Zhang, Haitao Guo, Jing Ren, Lukas Strizik, Tomas Wagner, Gerald Farrell, Pengfei Wang, Ultrabroadband mid-infrared emission from Cr2+-doped infrared transparent chalcogenide glass ceramics embedded with thermally grown ZnS nanorods, Journal of the European Ceramic Society, Volume 39, Issue 11, 2019, Pages 3373-3379, ISSN 0955-2219, DOI: 10.1016/j.jeurceramsoc.2019.04.048.

This Article is brought to you for free and open access by the Photonics Research Centre at ARROW@TU Dublin. It has been accepted for inclusion in Articles by an authorized administrator of ARROW@TU Dublin. For more information, please contact arrow.admin@tudublin.ie, aisling.coyne@tudublin.ie, vera.kilshaw@tudublin.ie.

Funder: National Key R&D Program of China; National Natural Science Foundation of China (NSFC); Fundamental Research Funds for the Central Universities; Harbin Engineering University; Natural Science Foundation of Heilongjiang Province of China

Authors

Xiaosong Lu, Zhiqiang Lai, Runan Zhang, Haitao Guo, Jing Ren, Lukas Strizik, Tomas Wagner, Gerald Farrell, and Pengfei Wang

This article is available at ARROW@TU Dublin: https://arrow.tudublin.ie/prcart/21

Journal of the European Ceramic Society 39 (2019) 3373–3379

Contents lists available at ScienceDirect

Journal of the European Ceramic Society

journal homepage: www.elsevier.com/locate/jeurceramsoc

Short communication

Ultrabroadband mid-infrared emission from Cr^{2+}-doped infrared transparent chalcogenide glass ceramics embedded with thermally grown ZnS nanorods

Xiaosong Lu[a], Zhiqiang Lai[a], Runan Zhang[a], Haitao Guo[b], Jing Ren[a,*], Lukas Strizik[c], Tomas Wagner[c,d], Gerald Farrell[e], Pengfei Wang[a,f,*]

[a] Key Lab of In-fiber Integrated Optics, Ministry Education of China, Harbin Engineering University, Harbin 150001, China
[b] State Key Laboratory of Transient Optics and Photonics, Xi'an Institute of Optics and precision Mechanics, Chinese Academy of Science (CAS), Xi'an, Shaanxi 710119, China
[c] Department of General and Inorganic Chemistry, Faculty of Chemical Technology, University of Pardubice, Studentska 573, 53210 Pardubice, Czech Republic
[d] Department of General and Inorganic Chemistry, Faculty of Chemical Technology and Center for Materials and Nanotechnologies, University of Pardubice, Studentska 573, Pardubice 532 10, Czech Republic
[e] Photonics Research Centre, Dublin Institute of Technology, Kevin Street, Dublin 8, Ireland
[f] Key Laboratory of Optoelectronic Devices and Systems of Ministry of Education and Guangdong Province, College of Optoelectronic Engineering, Shenzhen University, Shenzhen, 518060, China

ARTICLE INFO

Keywords:
Mid-infrared (MIR) emission
Chalcogenide glass
Glass ceramics

ABSTRACT

We report, for the first time to our knowledge, an ultrabroadband mid-infrared (MIR) emission in the range of 1800–2800 nm at room temperature from a Cr^{2+}-doped chalcogenide glass ceramic embedded with pure hexagonal (wurtzite) β-ZnS nanorods and study the emission-dependent properties on the doping concentration of Cr^{2+}. A new family of chalcogenide glasses based on $(100 - x)\ Ge_{1.5}As_2S_{6.5} - x$ ZnSe (in mol.%) was prepared by melt-quenching method. The Cr^{2+}: β-ZnS nanorods of ~150 nm in diameter and ~1 μm in length were grown in the Cr^{2+}-doped glass after thermal annealing. The compositional variations of glass structures and optical properties were studied. The crystalline phase, morphology of the thermally grown nanorods, and the microscopic elemental distributions were characterized using advanced nanoscale transmission electron microscopy analyses.

1. Introduction

Broadband and tunable mid-infrared (MIR, 2–5 μm) light sources are indispensable for a variety of applications including but certainly not limited to molecular spectroscopy, environmental monitoring, and non-invasive medical diagnostics [1]. Divalent transition metal ions (TM^{2+}: e.g., Cr^{2+}/Fe^{2+} etc.) doped II—VI chalcogenide (ChG) semiconductors (e.g., ZnS/Se etc.) have emerged as excellent MIR gain media, thanks to the following advantages including: ultrabroadband emission in the range of 2–5 μm, large stimulated emission cross-section (~10^{-18} cm^2), high quantum efficiency (> 70%) and being readily accessible to a number of commercially available pump sources (e.g., Er^{3+} or Tm^{3+} doped high power fiber lasers) [1–4]. Breathtaking progress has been made in the development of MIR lasers based on Cr^{2+} doped ZnS/Se crystals such that high-power (> 10 W) continuous and ultra-short pulsed (< 50 fs) MIR lasers have been realized [3].

However, the thermal lensing effect due to the relatively large thermo-optic coefficient of the TM^{2+}: II–VI crystals poses a serious constraint to laser beam quality and output power upscaling. The use of waveguide structures (e.g., in plane or fiber form) obtained by incorporating Cr^{2+}: ZnS/Se crystals in glass hosts to confine the mode propagation could be a viable solution to this problem [5–8]. Such a "phosphor-in-glass" strategy demands for compatibility between the materials properties such as refractive index matching. In this respect, chalcogenide glasses (ChGs) are ideal materials of choice because of large refractive indices (> 2.0) that can be varied in a large space on demand, excellent IR transparency (up to 8 μm in sulfide glasses) and relatively low melting temperatures that are necessary for the minimum corrosion on the incorporated II–VI crystalline powders [5,6,9]. Both theoretical and experimental studies have demonstrated the lasing feasibility of the Cr^{2+}: ZnS/Se powders in ChGs [5,10]. Of particular interest is the demonstration of random lasing (RL) based on the Cr^{2+}:

* Corresponding authors at: Key Lab of In-fiber Integrated Optics, Ministry Education of China, Harbin Engineering University, Harbin 150001, China.
E-mail addresses: ren.jing@hrbeu.edu.cn (J. Ren), pengfei.wang@dit.ie (P. Wang).

https://doi.org/10.1016/j.jeurceramsoc.2019.04.048
Received 19 March 2019; Received in revised form 25 April 2019; Accepted 26 April 2019
Available online 28 April 2019
0955-2219/ © 2019 Elsevier Ltd. All rights reserved.

ZnSe/ChG glass composites, which opens the way for the design of MIR-active fiber lasers at low costs [5]. Random lasing has been realized from both the Cr^{2+}: ZnS/Se micro- and nano-crystals (NCs) so far [11,12].

Previously, the incorporation of II–VI crystals in ChGs has been realized by two ways: a) low temperature melt-quenching [5,6], and b) hot-pressing of II–VI crystalline powders with ChG glassy powders in vacuum [8,13]. However, the former suffers from corrosion of the II–VI powders especially when the composites were prepared at high temperatures, causing serious PL quenching and even total de-activation of the TM^{2+} dopants [8]. As such, only those ChGs with low melting temperatures have been used as the host glasses (e.g., As—S, As—S—Se), imposing considerable constraints on the compositional choices of ChGs. The latter, on the other hand, is susceptible to uncontrollably high optical losses due to the porosity nature of the hot-pressed composites [13]. Very recently, capitalizing on the metastable characteristic of glasses, we have proposed a new preparation method of II–VI crystal/ChG glass ceramic composites based on the nucleation and crystallization mechanism of ChGs [14,15]. It has been demonstrated that ZnS NCs (< 100 nm) can be grown in the As_2S_3-ZnSe glass system upon controlled thermal annealing [14]. The ZnS NCs/As_2S_3 glass ceramic composites thus obtained retain good IR transparency, and are expected to have limited optical losses [5,8]. However, the low solubility of ZnSe (< 5 mol.%) in As_2S_3 sets an upper limit of the crystallinity of II-VI crystals, which appears to be a disadvantage in terms of the number of MIR-active tetrahedral crystalline sites (viz., Zn^{2+} sites) indispensable for Cr^{2+} emissions.

In the present work, a new glassy host is designed based on the $(100 - x)Ge_{1.5}As_2S_{6.5} - x$ ZnSe (in mol.%) system, which allows for the incorporation of a much larger content of the ZnSe compound (~15 mol.%) before glass optical properties start to degrade [6]. The composition was chosen taking into account of the following points: a) The $Ge_{1.5}As_2S_{6.5}$ is extremely thermally stable (no crystallization peak) as it lies at the center of the glass forming region of the Ge—As—S system [16], and b) ZnSe can be more readily resolved in ChGs as compared with ZnS. The latter with an extremely high melting temperature (1850 °C) cannot be completely melted at the typical ChGs synthesize temperatures (< 1000 °C). Melting at higher temperatures is not allowed by the softening temperature (1100 °C) of the silica glass tube, and the very explosive nature of the glass preparation [14].

This article is arranged in such a way that in the beginning, glass forming ability, structure, and basic optical properties (including IR transmission and refractive index) are characterized as a function of the ZnSe content, and once the suitable base glass composition is found, the Cr^{2+}-doped glass samples are prepared and their photoluminescence (PL) properties are studied.

2. Experiments

The base glasses were prepared by traditional melt-quenching method: raw materials (Ge, As, S with 5N-purity, and ZnSe, $CrCl_2$ with 4N-purity) were weighed according to the compositions: $(100 - x)Ge_{1.5}As_2S_{6.5} - x$ ZnSe (x = 0, 10, 15, 20, 30, in mol.%) and $85Ge_{1.5}As_2S_{6.5} - 15ZnSe - 0.3CrCl_2$, and then melted at 950 °C for 12 h in an evacuated (10^{-3} Pa) silica glass tube. The 950 °C melts were quenched in water and then thermally annealed at 180 °C for 5 h. The annealing temperature and time were set both for releasing inner stress and inducing crystallization in the glass. To avoid oxidization of Cr^{2+}, the weighing of the raw materials was carried out in a glove box purged with inert gas, and the thermal annealing was also implemented under vacuum.

The crystalline phase of the thermally grown NCs was measured using an X-ray diffractometer (XRD, D/MAX 2550VB/PC, Rigaku Corporation, Japan) with the Cu-Kα irradiation. The microscopic morphology, particle size and distribution of the NCs were examined by high angle annular dark field scanning TEM (HAADF-STEM) using FEI Talos F200x, USA, operating at 200 kV and equipped with an energy-dispersive spectrometer (EDS) system. The elemental mapping was measured in the STEM-EDS mode [17]. TEM samples were prepared by manual grinding to 200 μm thick and then processed by ion beam milling technique (PIPS II system from GATAN) to about 40 nm thick [18]. The glass structure was investigated by Raman spectra using a Renishaw in Via Raman microscope (Renishaw, Gloucestershire, UK) at an excitation wavelength of 532 nm. The glass transition and crystallization temperatures were extracted from the DSC curves obtained using a TA D2000 (New Castle, DE) under non-isothermal conditions from room temperature to about 500 °C (773 K) with a linear ramp heating rate of 10 K/min. X-ray photoelectron spectroscopy (XPS) was measured by a Thermo Fisher Scientific ESCALAB 250Xi spectrometer with an Al $K\alpha$ X-ray source ($h\nu$ = 1253.6 eV). The binding energies were referenced to the C 1s peak (E_b = 284.6 ± 0.1 eV).

Optical transmission spectra were measured by a Perkin-Elmer Lambda 950 UV-VIS spectrophotometer from 500 to 2500 nm and by a Bruker Tensor 27 Fourier transform infrared spectrophotometer (FTIR, Ettlingen, Germany) from 2.5 to 15 μm. Mid-infrared refractive indices were measured using an infrared variable angle spectroscopic ellipsometer (IR-VASE, J. A. Woollam Co.) with rotating analyzers. PL spectra were measured by an Edinburgh FLS980 fluorescence spectrometer (Edinburgh Instruments), with the PL intensity corrected by the instrumental response. The excitation source is a 1550 nm erbium-doped fiber laser.

3. Results and discussion

As shown in Fig. 1, the samples remain completely amorphous until

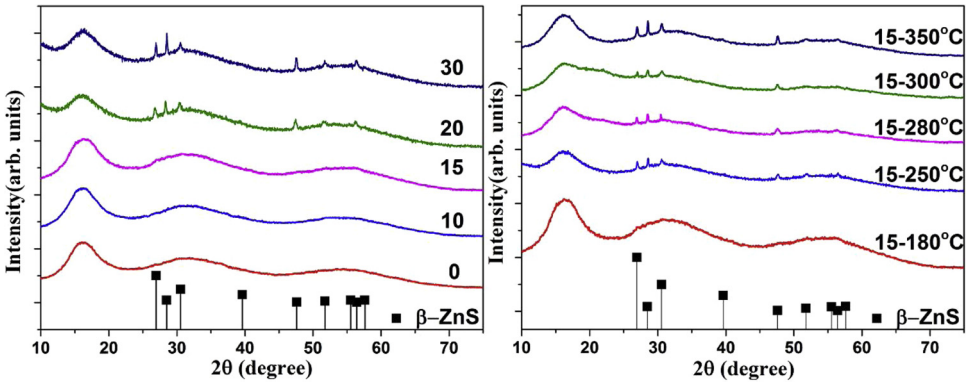

Fig. 1. XRD patterns of (a) the $(100 - x)$ $Ge_{1.5}As_2S_{6.5} - x$ ZnSe (x = 0, 10, 15, 20, 30, in mol.%) samples annealed at 180 °C, and (b) the $85Ge_{1.5}As_2S_{6.5} - 15ZnSe$ sample annealed at different temperatures. Standard hexagonal β-ZnS crystal is shown at the bottom (JCPDF card No. 36-1450).

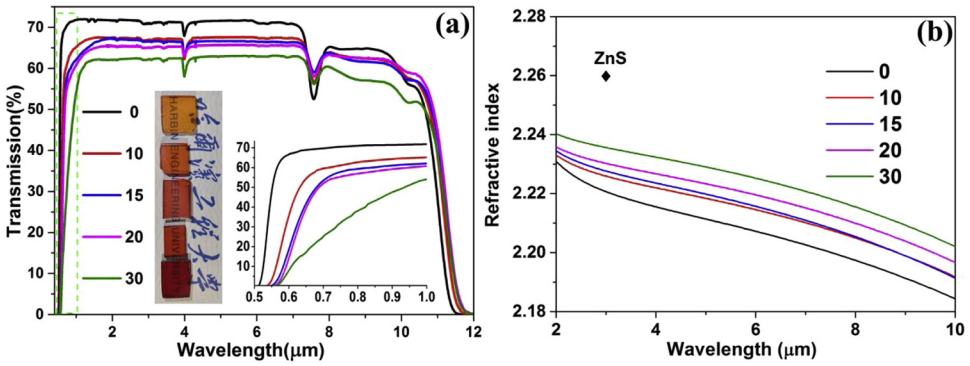

Fig. 2. (a) Transmission spectra and (b) refractive index dispersion curves of the samples $(100 - x)$ $Ge_{1.5}As_2S_{6.5} - x$ ZnSe (x = 0, 10, 15, 20, 30, in mol.%) with a thickness of 2.0 mm. Insets in (a) are the digital photo of the samples and the expanded part of the spectra in the short cut-off wavelength. The diamond in (b) indicates the refractive index of ZnS crystal at 3 μm [4].

the ZnSe content increases up to 15 mol.% as reflected by the featureless broad XRD patterns. Further increase in the ZnSe content results in the precipitation of pure hexagonal β-ZnS crystal according to the appearance of sharp diffraction peaks (JCPDF card No. 36-1450). The result indicates that approximately 15 mol.% ZnSe can be added in the designed $Ge_{1.5}As_2S_{6.5}$ glass host before crystallization. The crystallinity (volume fraction of the crystalline phase) in samples with larger ZnSe contents (e.g., ≥ 20 mol.%) is about 4% as estimated by the ratio of the area under the indexed crystallographic peaks to that under the whole XRD patterns. The crystallinity is larger by more than four times of that achieved in the As_2S_3-ZnSe system (less than 1%) [14]. Larger crystallinities are favored for accommodating more MIR-active Cr^{2+} ions and thus exhibiting stronger MIR PL, albeit at the expense of optical transparency (Fig. 2).

The effect of annealing temperature on crystallization behavior was studied using $85Ge_{1.5}As_2S_{6.5} - 15$ZnSe as an example. For this sample, crystallization takes place only when the annealing temperature is raised up to 250 °C. Comparing the intensities and bandwidths of the diffraction bands corresponding to the β-ZnS crystal, it can be known that the size and amount of the thermally grown crystals do not suffer from significant changes in the temperature range of 250–350 °C, which can be accounted for by the diffusion-limited crystallization as will be discussed below.

For bulk materials, the more thermodynamically stable ZnS phase below 1020 °C is the cubic one. However, it has been proved that stable wurtzite phase can also exist for NCs synthesized at temperatures even below 400 °C [19]. Although the exact mechanisms remain controversial, that NCs contain much few stable defects have been assumed to serve as nucleation sites for phase transformations. Besides, morphology of the NCs also influences their phase stability. For example, ZnS nanobelts are extremely stable in the wurtzite phase at low temperatures [20]. The formation of β-ZnS in the studied GCs may be understood with respect to the shape similarities between nanobelts reported previously and nanorods obtained in this work.

The optical transmission spectra of the samples are shown in Fig. 2(a). The samples are homogenous and visible-light transmitting even for the partially crystallized sample with the largest amount of ZnSe (30 mol.%, inset photo in Fig. 2(a)). They also exhibit good IR transparency in the range of 2–8 μm. The overall transmission decreases with the ZnSe content owing to the increased reflection as it is proportional to the refractive index according to the Fresnel formula [14]. As shown in Fig. 2(b), addition of the heavy ZnSe compound (density = 5.26 g/cm^3 [4]) raises the refractive index of the glass. The refractive indices of the ZnS and ZnSe crystals are 2.26 and 2.44 [4], respectively, therefore from the refractive index matching point of view, samples with a larger content of ZnSe are preferred. However, pronounced transmission losses especially in the visible and near-infrared (NIR) wavelength region happens at large contents of ZnSe (e.g, > 20 mol.%, inset in Fig. 2(a)). Benefiting from the broad glass forming region of the Ge-As-S system, it is possible to have an optimized index matching by tuning the glass composition, for example, increasing the Ge content [21].

Both the short (inset in Fig. 2(a)) and long cut-off wavelengths of the samples suffer from a red-shift towards longer wavelengths with the ZnSe content. The short cut-off wavelength is subject to the average electron affinity of anions and bond energy of the glass. It decreases with decreasing affinity of anions (200 and 195 kJ/mol for S and Se, respectively). The long cut-off wavelength, on the other hand, is proportional to the average phonon energy of the glass, which decreases with the ZnSe content as will be illustrated by Raman spectra shown below (Fig. 4).

The characteristic glass transition temperature T_g which reflects the network rigidity was measured for the samples as shown in Fig. 3. An increasing tendency of T_g with the ZnSe content can be found. The variation of T_g can be accounted for by the Gibbs and DiMarzio model as [22]:

$$Tg = \frac{T_0}{[1 - \beta(< r > - 2)]} \quad (1)$$

where T_0 is the glass transition temperature of the pure polymer-like chain (e.g., S—S chains), β is a system-dependent constant, $< r >$ is the average coordination number (CN) of the network. Such model predicts an increase in T_g with $< r >$, which has indeed been confirmed by many studies of ChGs provided that no phase separation is present [23,24]. It has been previously validated by extended X-ray-absorption final structure (EXAFS) study that zinc, the same as germanium, tends to be four-fold coordinated in ChGs [25], and thus has a larger CN than the three-fold coordinated arsenic. Consequently, addition of ZnSe leads to the increase in $< r >$ and T_g. At the largest ZnSe content (30 mol.%), however, T_g decreases, possibly due to the formation of Se_8 molecular groups that tend to destroy the backbone of the network and

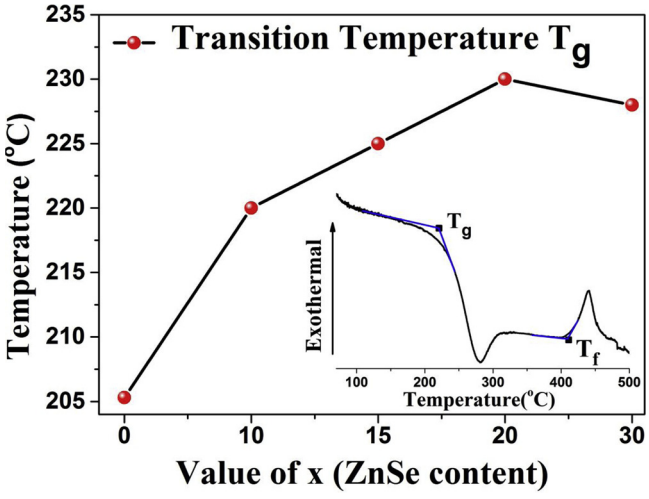

Fig. 3. Variation of glass transition temperature (T_g) with the ZnSe content (x). Inset: DSC curve of the $85Ge_{1.5}As_2S_{6.5} - 15$ZnSe sample taken as an example.

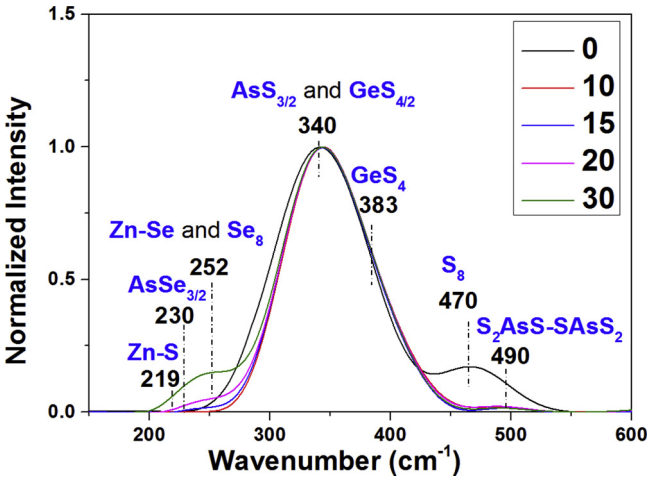

Fig. 4. Reduced Raman spectra of the samples $(100 - x)$ $Ge_{1.5}As_2S_{6.5} - x$ ZnSe (x = 0, 10, 15, 20, 30 mol.%) normalized with respect to the 340 cm^{-1} band. Also shown are the assignments to separate bands.

thus causing a decrease in T_g (Fig. 3) [24]. (c.f. Raman spectra shown below, Fig. 4).

Reduced Raman spectra of the samples (free of thermal population effects [26]) were measured to understand the variations of glass structure (Fig. 4). The spectra below 200 cm^{-1} could not be measured owing to the large undesirable background scattering. The spectra mainly consist of four broad bands centered at ~252, 340, 470 and 490 cm^{-1}. The 252 cm^{-1} band involves overlapping of several vibrational modes including the Zn-Se (252 cm^{-1}), $AsSe_{3/2}$ pyramids (230 cm^{-1}), Se_8 rings (250 cm^{-1}), and Zn-S units (219 and 273 cm^{-1}) [24,27]; The 340 cm^{-1} band contains contributions from the $AsS_{3/2}$ pyramids (335 cm^{-1}), and GeS_4 (342 cm^{-1} and 383 cm^{-1}) tetrahedra [23]; The 470 cm^{-1} band stems from the S_8 rings [23]; The 490 cm^{-1} band can be assigned to the $S_2AsS–SAsS_2$ units [23]. Because of the strong overlapping of Raman peaks, a quantitative analysis by fitting the Raman spectra using multi-peaks deconvolution proved to be unsuccessful. Even so, general trends can be clearly noticed as the ZnSe content increases: a) the 470 cm^{-1} band intensity drops dramatically, b) the 252 cm^{-1} band intensity grows gradually, and c) the 340 cm^{-1} band slightly shifts to longer wavenumber (from 340 to 345 cm^{-1}). The results point out that the addition of ZnSe facilitates the formation of the Zn—Se, As—Se and Zn—S bonds at the expense of the As—S and S—S bonds [14].

Although the glasses were free of crystallization when the ZnSe content was no more than 15 mol.% (Fig. 1), the addition of Cr^{2+} (0.3 mol.%) caused significant crystallization with a large crystallinity (~ 5%) after annealing at 180 °C for 5 h. Both the XRD (Fig. 5(a)) and TEM (Fig. 5(b)–(d)) measurements confirm that the precipitated crystals are pure wurtzite β-ZnS. The thermally grown β-ZnS crystals are in the nanorod shape of ~150 nm in diameter and ~1 μm in length (Fig. 5(b)), and free of structural defects (Fig. 5(c)). The particle size is larger than previously found in As_2S_3 ChGs (~100 nm) [17], however, it is considerably smaller than in samples prepared by the phosphor-in-glass method (several micrometers) [5,6]. Smaller particle sizes are favored for reduced optical losses. Such a limited growth of β-ZnS crystals can be understood according to the microscopic distributions of the elements in the sample as discussed below.

HAADF-STEM image of the Cr^{2+}-doped sample, and its corresponding STEM-EDS elemental mappings are given in Fig. 6. The enrichment of the Zn (Fig. 6(b)) and Cr (Fig. 6(c)) elements in the precipitated particles provides straightforward evidence of formation of ZnS: Cr^{2+} nanorods. Sulfur is homogeneously distributed (Fig. 6(d)), while the distributions of the Ge (Fig. 6(e)), As (Fig. 6(f)) and Se (Fig. 6(g)) elements are complementary to the Zn element. In other words, the ZnS: Cr^{2+} nanorods are surrounded by a glassy layer rich in Ge, As and Se. The crystal growth may be inhibited by a diffusion barrier of the highly viscous, germanium and arsenic-enriched shell [17,28].

Thanks to the limited crystallization, the sample retains good IR transparency and more importantly shows the unique ultrabroadband MIR emission of Cr^{2+} as shown in Fig. 7. The IR transparency of the sample is much greater than obtained by the hot-pressing method (less than 40%) [8]. However, the $CrCl_2$ doping results in decreased transmission, particularly in the visible and NIR wavelength region (0.6–2 μm), because of the enhanced crystallization tendency upon the $CrCl_2$ doping. For random lasing application, a balanced degree of scattering between crystal grains is required for stimulated emission [12,29]. Because of the strong scattering, we failed to record the weak absorption band of Cr^{2+} due to the $^5T_2 \rightarrow {}^5E$ transition, as such absorption band of ZnS: Cr^{2+} reported previously is shown for demonstration (Fig. 7(a)) [3]. The valence state of Cr was investigated by XPS measurement as shown in Fig. 7(b). According to the XPS spectrum of the 0.3 mol.% $CrCl_2$ doped sample, the binding energy of the Cr 2p3/2 peak is located at 573.8 eV, closely resembling that of Cr^{2+} doped ZnSe (573.6 eV) [30], however, less than that of Cr_2S_3 (575.6 eV) and Cr_2Se_3 (574.5 eV) [31]. The result points out clearly that the dominating valence state of Cr in the studied samples is Cr^{2+}. In our previous studies, it was found that ChGs were quite different from their oxide counterparts in that, they tended to provide a weak reducing chemical environment such that multi-valence dopants such as Mn, Eu and Bi ions could exist in their low valence states like Mn^{2+}, Eu^{2+} and Bi^{+} which is benefited from the weak reducing atmosphere during glass synthesis [32]. Besides, those Cr^{2+} ions incorporated in the ZnS nanorods may be protected by the rigid structure of ZnS, and thus become less sensitive to the outer oxidation environments.

The broad absorption band of Cr^{2+} peaking at 1690 nm promises a number of viable pumping strategies such as using Er^{3+} or Tm^{3+} doped high-power fiber lasers [3]. Here, a 1570 nm Er^{3+}-doped fiber laser was used as the pump source. An ultrabroadband MIR emission in the range of 1800–2800 nm is observed at room temperature from the ChG glass ceramic embedded with the ZnS: Cr^{2+} nanorods. The emission intensity increases with the $CrCl_2$ concentration until 0.3 mol.%, and concentration quenching occurs at the higher doping content of 0.5 mol.%. The emission is from the $^5E \rightarrow {}^5T_2$ spin-allowed transition of tetrahedrally coordinated Cr^{2+} ions (Fig. 7(c)). The emission band of the sample investigated in this work closely resembles that of the hot-pressed ZnS: Cr^{2+} transparent ceramics of particle sizes of 100–200 nm [33]. The broad emission band of Cr^{2+} covers several characteristic emission bands of RE ions such as the 1.8 μm of Tm^{3+} [17], and 2.1 μm of Ho^{3+} [34], and partially covers the 2.7 μm of Er^{3+} [35]. This, together with the easy materialization of waveguiding based on ChGs [35,36], offers the sample with the potential of being used as a MIR light source for chemical sensing applications [35].

4. Conclusion

A new family of ChGs based on the $(100 - x)$ $Ge_{1.5}As_2S_{6.5} - x$ ZnSe system is found. As high as 15 mol.% ZnSe can be added in the glass without crystallization, and the resulting glass maintains good IR transparency. The addition of ZnSe leads to the formation of the Zn—Se, As—Se and Zn—S bonds at the expense of the S—S and As—S bonds, and the increase in the glass transition temperature as well as the refractive index. The $CrCl_2$ doping facilitates the formation of the ZnS nanorods after annealing at 180 °C for 5 h. The valence state of Cr is dominated by Cr^{2+} ions which are well incorporated in the ZnS nanorods. The growth of the ZnS: Cr^{2+} nanorods is inhibited by a diffusion barrier of the germanium and arsenic-enriched glassy shell. Using a 1570 nm Er^{3+}-doped fiber laser as the pump source, an ultrabroadband MIR emission in the range of 1800–2800 nm is observed at room temperature for the first time, with an optimized $CrCl_2$ doping concentration at 0.3 mol.%.

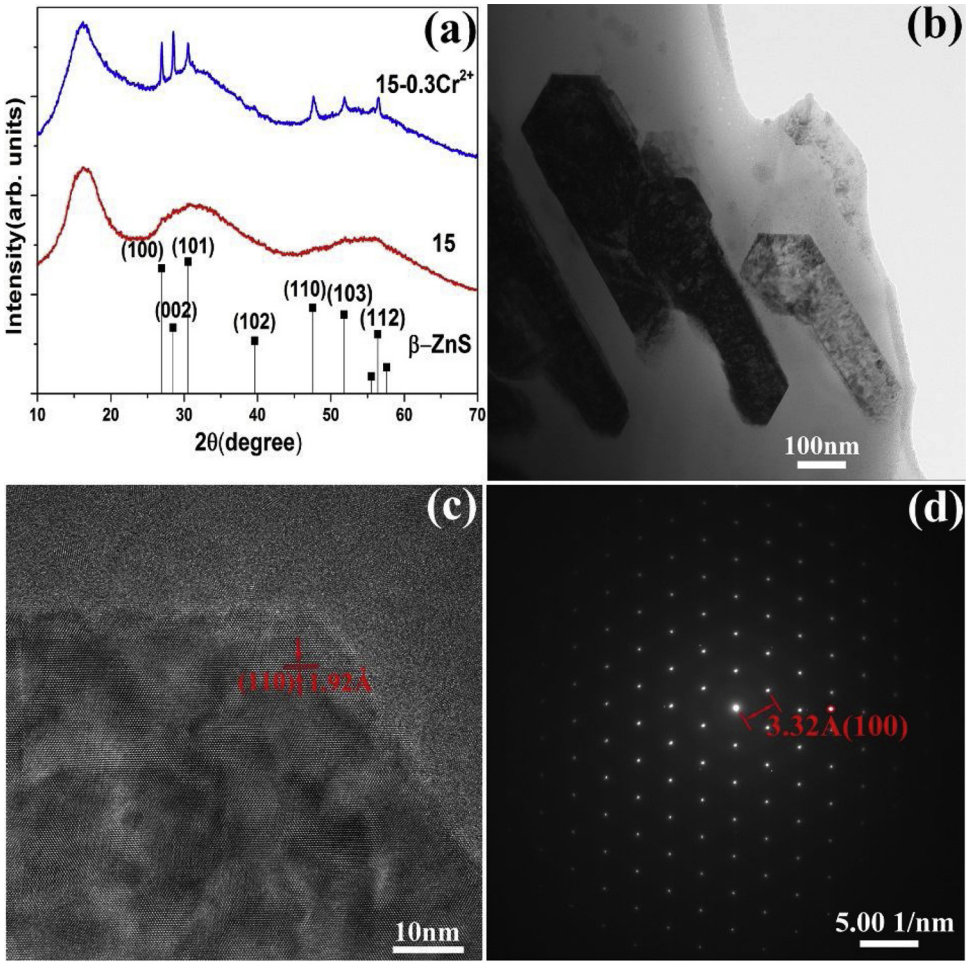

Fig. 5. (a) XRD patterns of the non-doped (15), 0.3 mol.% Cr^{2+}-doped (15-0.3Cr^{2+}) samples and the standard β-ZnS crystal; (b) Dark field TEM, (c) HRTEM images and (d) selected area diffraction pattern of the 0.3 mol.% Cr^{2+}-doped sample. The d-spacing and corresponding crystal lattice direction are shown in (c) and (d).

Acknowledgements

This work was financial supported by National Key R&D Program of China (2016YFE0126500), National Natural Science Foundation of China (NSFC61575050, 51872055and61475189), the Fundamental Research Funds for the Central Universities (HEUCFG201841), Key Program for Natural Science Foundation of Heilongjiang Province of China (ZD2016012), the Open Fund of the State Key Laboratory on Integrated Optoelectronics (IOSKL2016KF03), Natural Science Foundation of Heilongjiang Province of China (F2017006), the 111 project (B13015) to the Harbin Engineering University, European Regional Development Fund-Project "High sensitive sensors and low density materials based on polymeric nanocomposites - NANOMAT (No. CZ.02.1.01/0.0/0.0/17_048/0007376)".

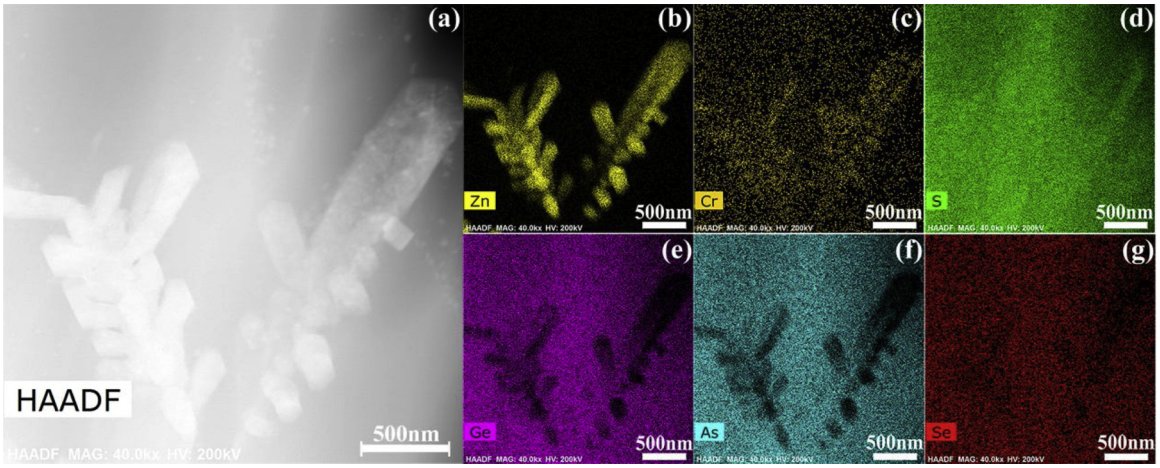

Fig. 6. (a) HAADF-STEM image of the 0.3 mol.% Cr^{2+} doped sample, and its corresponding STEM-EDS elemental mappings of (b) Zn, (c) Cr, (d) S, (e) Ge, (f) As, (g) Se, with their concentrations reflected by the brightness in colors.

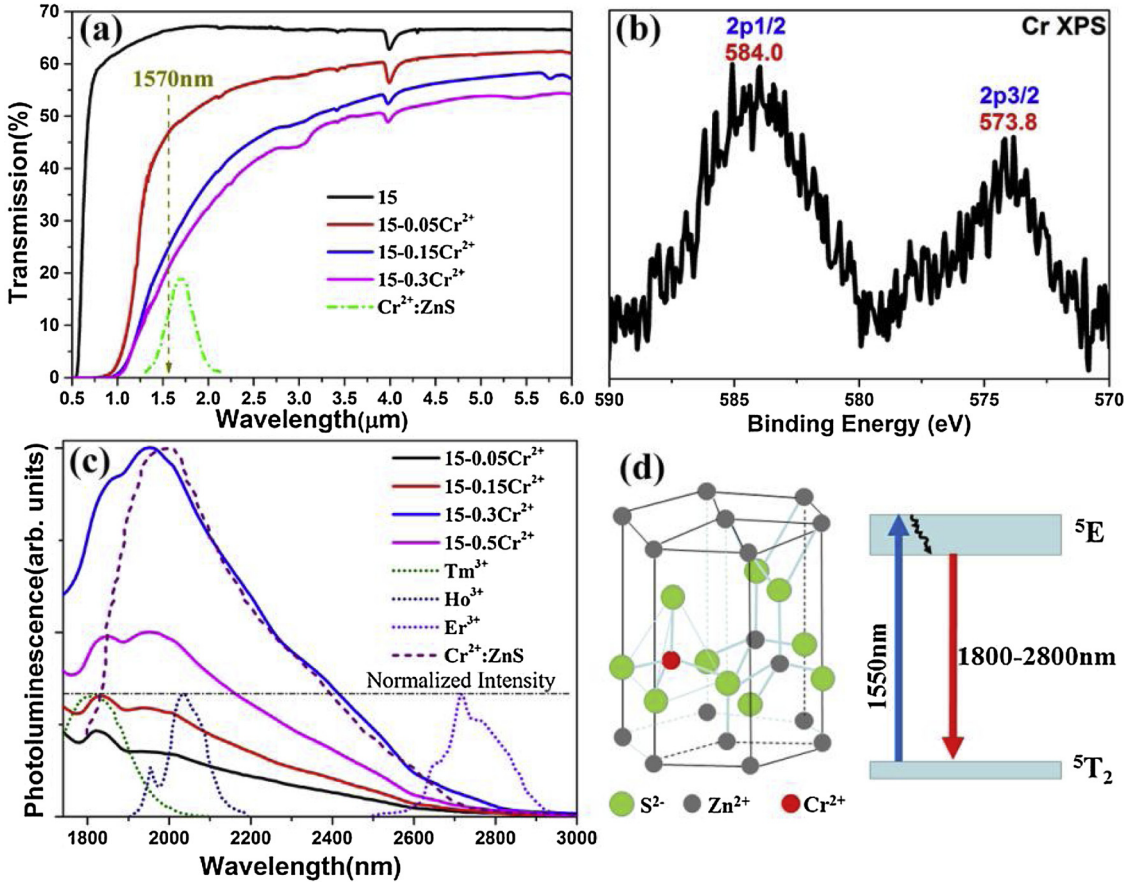

Fig. 7. Transmission (a) and MIR emission (c) spectra of the non-doped (15) and x mol.% Cr^{2+}-doped ($15 - xCr^{2+}$: x = 0.05, 0.15, 0.3, 0.5) samples. The excitation is the 1570 nm Er^{3+}-doped fiber laser (0.6 W). Inset in (a) is the characteristic absorption band of ZnS: Cr^{2+} crystal [3]. The characteristic emission spectra of ZnS: Cr^{2+} crystal and some selected rare-earth ions [17,34,35] are also included in (c). (b) XPS spectrum of the 0.3 mol.% Cr doped sample. (d) Crystal structure of Cr^{2+}-doped wurtzite β-ZnS nanocrystal, and electronic states responsible for the MIR emission.

References

[1] E. Sorokin, S. Naumov, I.T. Sorokina, Ultrabroadband infrared solid-state lasers, IEEE J. Sel. Top. Quantum Electron. 11 (3) (2005) 690–712.

[2] S.B. Mirov, I.S. Moskalev, S. Vasilyev, V. Smolski, V.V. Fedorov, D. Martyshkin, J. Peppers, M. Mirov, A. Dergachev, V. Gapontsev, Frontiers of mid-IR lasers based on transition metal doped chalcogenides, IEEE J. Sel. Top. Quantum Electron. 24 (5) (2018) 1–29.

[3] S.B. Mirov, V.V. Fedorov, D. Martyshkin, I.S. Moskalev, M. Mirov, S. Vasilyev, Progress in mid-IR lasers based on Cr and Fe-doped II–VI chalcogenides, IEEE J. Sel. Top. Quantum Electron. 21 (1) (2015) 292–310.

[4] S. Mirov, V. Fedorov, I. Moskalev, D. Martyshkin, C. Kim, Progress in Cr^{2+} and Fe^{2+} doped mid-IR laser materials, Laser Photonics Rev. 4 (1) (2010) 21–41.

[5] D.V. Martyshkin, J.T. Goldstein, V.V. Fedorov, S.B. Mirov, Crystalline Cr^{2+}: ZnSe/chalcogenide glass composites as active mid-IR materials, Opt. Lett. 36 (9) (2011) 1530–1532.

[6] E.V. Karaksina, V.S. Shiryaev, L.A. Ketkova, Preparation of composite materials for fiber optics based on chalcogenide glasses containing ZnS(ZnSe):Cr(2+) crystals, J. Non-Cryst. Solids 377 (2013) 220–224.

[7] J.R. Sparks, R. He, N. Healy, M. Krishnamurthi, A.C. Peacock, P.J.A. Sazio, V. Gopalan, J.V. Badding, Zinc selenide optical fibers, Adv. Mater. 23 (14) (2011) 1647–1651.

[8] A. Yang, J. Qiu, J. Ren, R. Wang, H. Guo, Y. Wang, H. Ren, J. Zhang, Z. Yang, 1.8–2.7 μm emission from As-S-Se chalcogenide glasses containing ZnSe: Cr2+ particles, J. Non-Cryst. Solids 508 (2019) 21–25.

[9] A. Ravagli, C. Craig, G.A. Alzaidy, P. Bastock, D.W. Hewak, Optical, thermal, and mechanical characterization of Ga_2Se_3-Added GLS glass, Adv. Mater. 29 (27) (2017) 1606329.

[10] M. Gorjan, M. Rochette, Theoretical study of continuous-wave lasing in Cr:ZnSe:glass composite waveguides, IEEE Photonics Conference 2012 (2012) 929–930.

[11] C. Kim, D.V. Martyshkin, V.V. Fedorov, S.B. Mirov, Mid-infrared Cr^{2+}:ZnSe random powder lasers, Opt. Express 16 (7) (2008) 4952–4959.

[12] G. Feng, C. Yang, S. Zhou, Nanocrystalline Cr^{2+}-doped ZnSe nanowires laser, Nano Lett. 13 (1) (2013) 272–275.

[13] B. Xue, B. Fan, X. Zhang, Y. Quiquempois, G. Martinelli, L. Calvez, The second-harmonic generation in chalcogenide glass-ceramic doped with CdS nanocrystals, Mater. Lett. 132 (2014) 130–133.

[14] X. Lu, Y. Zhang, J. Ren, E. Lewis, G. Farrell, A. Yang, Z. Yang, P. Wang, Chalcogenide glasses with embedded ZnS nanocrystals: potential mid-infrared laser host for divalent transition metal ions, J. Am. Ceram. Soc. 101 (2) (2017) 666–673.

[15] C. Lin, C. Rüssel, S. Dai, Chalcogenide glass-ceramics: functional design and crystallization mechanism, Prog. Mater. Sci. 93 (2018) 1–44.

[16] J.D. Musgraves, P. Wachtel, B. Gleason, K. Richardson, Raman spectroscopic analysis of the Ge–As–S chalcogenide glass-forming system, J. Non-Cryst. Solids 386 (2014) 61–66.

[17] X. Lu, Z. Lai, J. Ren, L. Strizik, T. Wagner, Y. Du, G. Farrell, P. Wang, Distribution of Tm^{3+} and Ni^{2+} in chalcogenide glass ceramics containing Ga_2S_3 nanocrystals: influence on photoluminescence properties, J. Eur. Ceram. Soc. 39 (7) (2019) 2580–2584.

[18] Z. Gao, X. Lu, Y. Chu, S. Guo, L. Liu, Y. Liu, S. Sun, J. Ren, J. Yang, The distribution of rare earth ions in a γ-Ga_2O_3 nanocrystal-silicate glass composite and its influence on the photoluminescence properties, J. Mater. Chem. C 6 (12) (2018) 2944–2950.

[19] F. Huang, J.F. Banfield, Size-dependent phase transformation kinetics in nanocrystalline ZnS, J. Am. Chem. Soc. 127 (12) (2005) 4523–4529.

[20] W. Zhongwu, L.L. Daemen, Z. Yusheng, C.S. Zha, R.T. Downs, W. Xudong, W.Z. Lin, R.J. Hemley, Morphology-tuned wurtzite-type ZnS nanobelts, Nat. Mater. 4 (12) (2005) 922–927.

[21] Y. Yang, Z. Yang, P. Lucas, Y. Wang, Z. Yang, A. Yang, B. Zhang, H. Tao, Composition dependence of physical and optical properties in Ge-As-S chalcogenide glasses, J. Non-Cryst. Solids 440 (2016) 38–42.

[22] A.N. Sreeram, D.R. Swiler, A.K. Varshneya, Gibbs-DiMarzio equation to describe the glass transition temperature trends in multicomponent chalcogenide glasses, J. Non-Cryst. Solids 127 (3) (1991) 287–297.

[23] Y. Yang, B. Zhang, A. Yang, Z. Yang, P. Lucas, Structural origin of fragility in Ge–As–S glasses investigated by calorimetry and Raman spectroscopy, J. Mater. Chem. B 119 (15) (2015) 5096–5101.

[24] R.P. Wang, A. Smith, A. Prasad, D.Y. Choi, B. Luther-Davies, Raman spectra of $Ge_xAs_ySe_{1-x-y}$ glasses, J. Appl. Phys. 106 (4) (2009) 043520.

[25] J. Choi, S.J. Gurman, E.A. Davis, Structure of amorphous Ge_xSe_{1-x} and $Ge_xSe_yZn_z$ thin films: an EXAFS study, J. Non-Cryst. Solids 297 (2) (2002) 156–172.

[26] Q. Hu, T. Wang, Y. Chu, X. Wang, Y. Du, J. Ren, X. Yang, G. Yang, X. Kong, P. Wang, Mixed alkali effects in Er^{3+}-doped borate glasses: influence on physical, mechanical, and photoluminescence properties, J. Am. Ceram. Soc. 00 (2019) 1–11.

[27] Q. Xiong, J. Wang, O. Reese, L.C. Lew Yan Voon, P.C. Eklund, Raman scattering from surface phonons in rectangular cross-sectional w-ZnS nanowires, Nano Lett. 4 (10) (2004) 1991–1996.
[28] Z. Gao, S. Guo, X. Lu, J. Orava, T. Wagner, L. Zheng, Y. Liu, S. Sun, F. He, P. Yang, J. Ren, J. Yang, Controlling selective doping and energy transfer between transition metal and rare earth ions in nanostructured glassy solids, Adv. Opt. Mater. 6 (13) (2018) 1701407.
[29] D.V. Martyshkin, V.V. Fedorov, C. Kim, I.S. Moskalev, S.B. Mirov, Mid-IR random lasing of Cr-doped ZnS nanocrystals, J. Opt. 12 (2) (2010) 024005.
[30] M. Shenasa, S. Sainkar, D. Lichtman, XPS study of some selected selenium compounds, J. Electron Spectrosc. Relat. Phenom. 40 (4) (1986) 329–337.
[31] E. Agostinelli, C. Battistoni, D. Fiorani, G. Mattogno, M. Nogues, An XPS study of the electronic structure of the $Zn_xCd_{1-x}Cr_2$(x = S, Se) spinel system, J. Phys. Chem. Solids 50 (3) (1989) 269–272.
[32] Q. Yan, R. Jing, G. Chen, CsCl modified Ge–Ga–S glasses codoped with Eu^{2+} and Mn^{2+}: a potential yellow phosphor for solid-state lighting, J. Am. Ceram. Soc. 95 (12) (2012) 3719–3721.
[33] Y. Li, Y. Liu, V.V. Fedorov, S.B. Mirov, Y. Wu, Hot-pressed chromium doped zinc sulfide infrared transparent ceramics, Scr. Mater. 125 (2016) 15–18.
[34] J. Ren, Y. Chu, Q. Hu, A. Yang, Z. Yang, Spectroscopic properties of Ce^{3+}/Yb^{3+}/Ho^{3+} triply doped bismuthate glasses, J. Alloys. Compd. 717 (2017) 171–176.
[35] J. Ari, F. Starecki, C. Boussard-Plédel, Y. Ledemi, Y. Messaddeq, J.L. Doualan, A. Braud, B. Bureau, V. Nazabal, Co-doped Dy^{3+} and Pr^{3+} $Ga_5Ge_{20}Sb_{10}S_{65}$ fibers for mid-infrared broad emission, Opt. Lett. 43 (12) (2018) 2893–2896.
[36] Q. Du, Z. Luo, H. Zhong, Y. Zhang, Y. Huang, T. Du, W. Zhang, T. Gu, J. Hu, Chip-scale broadband spectroscopic chemical sensing using an integrated supercontinuum source in a chalcogenide glass waveguide, Photon. Res. 6 (6) (2018) 506–510.